DISTRIBUTED KINETICS OF THE CHARGE MOVEMENTS IN BACTERIORHODOPSIN: EVIDENCE FOR CONFORMATIONAL SUBSTATES

M. HOLZ, M. LINDAU, AND M. P. HEYN
Biophysics Group, Department of Physics, Freie Universität Berlin, D-1000 Berlin 33, FRG

ABSTRACT The flash-induced charge movements during the photocycle of light-adapted bacteriorhodopsin in purple membranes attached to a black lipid membrane were investigated under voltage clamp and current clamp conditions. Signal registration ranged from 200 ns to 30 s after flash excitation using a logarithmic clock, allowing the equally weighted measurement of the electrical phenomena over eight decades of time. The active pumping signals were separated from the passive system discharge on the basis of an equivalent circuit analysis. Both measuring methods were shown to yield equivalent results, but the charge translocation could be accurately monitored over the whole time range only under current clamp conditions. To describe the time course of the photovoltage signals a model based on distributed kinetics was found to be more appropriate than discrete first order processes suggesting the existence of conformational substates with distributed activation energies. The time course of the active charge displacement is characterised by a continuous relaxation time spectrum with three broad peaks plus an unresolved fast transient (<0.3 μs) of opposite polarity. The time constants and relative amplitudes (in brackets) derived from the peak rate constants and relative areas of the three bands are: τ_1 = 32 μs (20%), τ_2 = 0.89 ms (15%) and τ_3 = 18 ms (65%) at 25°C in 150 mM KCl at pH7. The Arrhenius plots of the peak rate constants were linear yielding activation energies of E_{A1} = 57 kJ/mol, E_{A2} = 52 kJ/mol, and E_{A3} = 44 kJ/mol. The electrical signal at 890 μs has no counterpart in the photocycle of bacteriorhodopsin suspensions. Fits with a sum of exponentials required 5 to 6 components and were not reproducible. Analysis of photoelectrical signals with continuous relaxation time spectra gave equally good fits with fewer parameters and were well reproducible.

INTRODUCTION

Bacteriorhodopsin (bR) in the purple membrane (PM) of *Halobacterium halobium* is a light driven proton pump (Stoeckenius et al., 1979). In order to understand its mechanism a variety of methods has been developed to investigate the time course of the electrical signals during the photocycle. To get net electrical signals from the vectorial charge movement the PM's have to be oriented. For this purpose purple membrane fragments were oriented in saline suspension by an electric field (Keszthelyi and Ormos, 1980), immobilized in a gel (Der et al., 1985), or spread on a heptane water interface (Trissl, 1983). Other methods are based upon attachment of PM or bR containing liposomes to collodion or teflon films (Drachev et al., 1978; Rayfield, 1983, 1985, 1986) separating two compartments of a saline-filled chamber. We have studied flash-induced photoelectric signals of PM fragments adsorbed to an artificial bilayer lipid membrane (Bamberg et al., 1979; Fahr, 1981; Fahr et al., 1981). In this system current measurements give no reliable information about the slower components of the active charge displacement due to their small amplitude. On the other hand fast transients in the μs range are markedly affected in amplitude since the passive discharge time constant is of the same order of magnitude. As will be shown here with voltage measurements, the passive system discharge components can be clearly separated from the bR pumping signal, giving equally weighted data on the charge displacement over a wide time range.

The data reported by different authors on the time constants and amplitudes of exponential components of the charge movement in bR are in poor agreement. Evaluation of our data with a sum of exponentials gave irreproducible results between different membranes under otherwise identical conditions.

The assumption of the existence of conformational substates in proteins leads to distributed activation energies and thus to distributed time constants as shown for ligand binding by myoglobin (Austin et al., 1975). Fluorescence decay data of proteins were interpreted with a spectrum of time constants (Alcala et al., 1987, *a* and *b*). The time course of charge movements in bovine rhodopsin was described with power laws, which correspond to distributed time constants (Lindau and Rüppel, 1983). The photocycle of halorhodopsin was analysed with a distributed kinetics model (Xie et al., 1986). For the photocycle of bR distributed thermal barriers rather than branching or back reactions were suggested (Varo and Keszthelyi,

1983). The decay of the M_{412}-photointermediate of bR is well described by a continuous relaxation time spectrum with two bands (Groma and Dancshazy, 1986). For the L to M transition a distributed kinetics model was found to be slightly superior to previous discrete models (Xie et al., 1985). The analysis of bR photovoltage with a Gaussian two-band spectrum was reported (Rayfield, 1986a). Conformational substates due to heterogeneity of protein–retinal interactions have been detected by FTIR measurements (Braunstein et al., 1987). Conformational changes during the photocycle of bR involving the peptide backbone have been reported (Marrero and Rothschild, 1987). Our results strongly suggest that data analysis with continuous relaxation time spectra gives in fact a more adequate description of the charge displacement in bR than models based on discrete first order kinetics and might explain the large discrepancies between the published data.

MATERIALS AND METHODS

The experimental set up has been described previously (Fahr, 1981; Fahr et al., 1981). Black lipid membranes (BLM) were formed in a Teflon cell filled with 20ml of standard saline (0.15 M KCl buffered with 5 mM HEPES at pH7), if not otherwise indicated. The membrane-forming solution contained 1% (wt/vol) L-1,2-diphytanoyl-3-phosphatidylcholine (Avanti Polar Lipids, Birmingham, AL.) and 0.025% (wt/vol) octadecylamine (Fluka, puriss.) in n-decane (Merck, for gas chromatography). The BLM was formed over a hole (diameter 0.8 or 1.5 mm) in a diagonal septum dividing the cell in two compartments at an angle of 45°. A window allowed visual control of the membrane thinning process through a low-magnification microscope. The temperature was controlled by a thermostat and continuously measured in the bathing solution with a thermistor. Photosignals were recorded with light-shielded Ag-AgCl electrodes (RC1, World Precision Instruments, New Haven, Conn.). The cell and all electrically sensitive parts were shielded by a Faraday cage. Purple membrane (PM) fragments were prepared from strain S9 and stored as aqueous suspension (5 mg/ml) at −20°C. For the experiments aliquots of 50 μl were diluted threefold in standard saline and sonicated for 7 min in a bath sonifier (Sonorex RK100H; Bandelin Elektronic, Berlin (W), FRG). After formation of a bilayer 50 μl of the PM suspension were added to one compartment (10 ml) under gentle stirring. In most experiments we started the measurements after 1 h when the photoresponse was maximal. Membranes were usually stable for several hours. Weak continuous white background illumination was provided for light adaptation of the bR. The PM adsorbed to the black membrane was excited at 568 nm by short light pulses (5 ns) from a rhodamine G6 filled dye laser (FL2001, Lambda Physik, Göttingen, FRG), which was pumped by an UV excimer laser (EM50, Lambda Physik). Only the central part of the beam was used and only the black area of the membrane and not the lipid torus was illuminated (diameter 0.5 or 1 mm). The flash entered through the bR-free compartment. The energy of the light pulse was variable up to 2 mJ/cm² through neutral density filters and was determined with a calibrated Joulemeter (J3, Molectron, Sunnyvale, CA). For photovoltage measurements the electrodes were connected to a DC-coupled electrometer using a 3554 OP AMP (Burr Brown, International Airport Industrial Park, Tucson, AZ) with a rise time of ~50 ns and 20-fold amplification. The input resistance of the amplifier could be selected by external shunt resistors. Photocurrents were measured with platinized platinum electrodes if not otherwise indicated and a current to voltage converter with the same OP AMP (conversion factor 10^7V/A with R_{in} = 100 Ohm) was used.

Due to the slow passive electrical discharge of the membrane system the photovoltage signals were measured up to several seconds. For this purpose an 8 bit 4096 data points transient recorder (Datalab DL912, Data Laboratories Ltd, Mitcham, Surrey, UK) was driven by a home-built external timebase delivering equally spaced clock pulses in eight free programmable consecutive time intervals from 200 ns to 30 s. The data were stored and averaged by a minicomputer (HP1000 Hewlett and Packard, Wolfe Read, Cupertino, USA). The time course of the signals was routinely evaluated graphically by plots with a logarithmic time scale. This kind of graphical representation (Trissl, 1983; Rayfield, 1985, 1986; Grzesiek and Dencher, 1986) is most suitable to display processes extending over several decades of time, since it allows rough evaluation by visual inspection. Points of inflection mark the time constants of exponential components and the slopes at these points give the relative amplitudes (Nagle, 1981). Fitting with the iterative least squares FORTRAN programs DISCRETE (Provencher, 1976, *a* and *b*) and CONTIN (Provencher, 1982, *a–c*) was done on a CDC185 to which the data were transferred through a data communication line. Both programs were tested with simulated data. The quality of the fits to our experimental data was routinely checked by plots of the residuals.

RESULTS

1. Photocurrent Measurements

Fig. 1*a* shows the typical photocurrent signal on a logarithmic time scale. It is similar to those published previously (Keszthelyi and Ormos, 1980; Fahr 1981; Fahr et al., 1981; Der et al., 1984) which were, however, displayed on a linear time scale. A transient limited by the risetime of the recording system (~0.3 μs) is followed by a slower component of opposite polarity with a time constant of ~3 μs, which is the passive system discharge component (Fahr et al., 1981). The current decays with a time constant of ~20 μs. Components with larger time constants cannot be detected by eye due to their small amplitude.

The pumped charge or a dipole change within bR can be interpreted by an induced image charge on the plates of the capacitance of the purple membrane. Under voltage clamp conditions the resulting current is proportional to the displacement velocity of the charge (Rayfield, 1983)

$$I = \frac{dq}{dt} = \frac{q}{d} \cdot \frac{dx}{dt} \text{ or } dq = \frac{q}{d} \cdot dx \qquad (1)$$

dx is the infinitesimal displacement normal to the membrane, d is the membrane thickness and q is the pumped charge. The time course of the displacement should thus be obtained directly from the integrated current signal. The signal of Fig. 1 *a* was integrated numerically after subtraction of the passive component and the result is shown in Fig. 1 *b*. A slower charge movement in the 20 ms range appears, but it is poorly resolved due to experimental noise. Current measurements are clearly not suitable for the time-resolved registration of the whole charge movement.

2. Photovoltage Measurements

Because of the lack of reliable information about the slower components of the charge movement in current signals and the direct proportionality between the voltage and the charge displacement, we mainly did photovoltage measurements. The typical time course of the photovoltage is shown in Fig. 1 *c*. The signal shows four points of

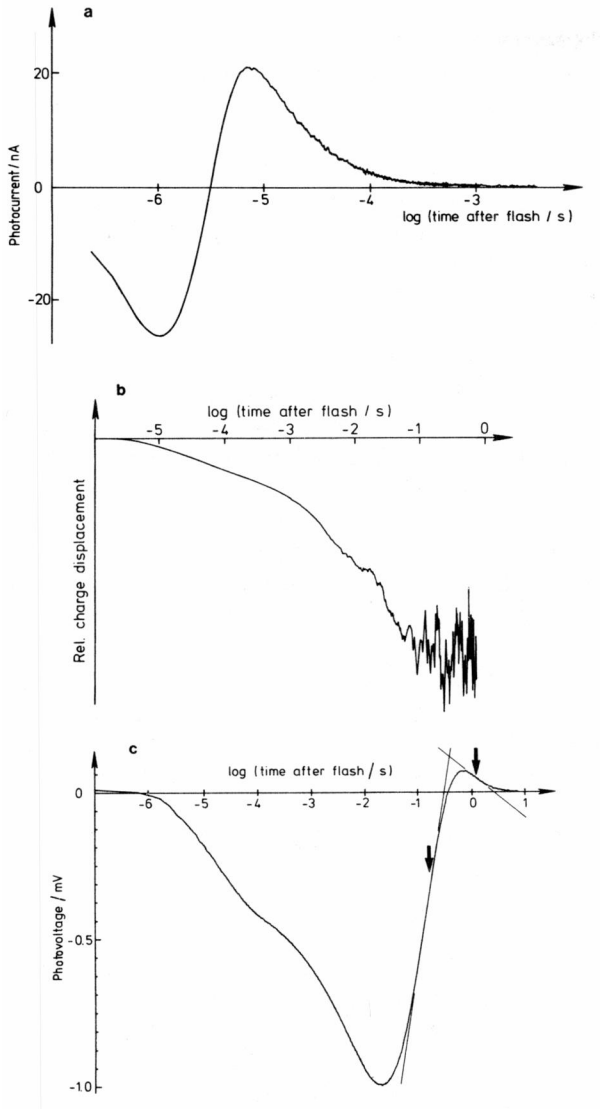

FIGURE 1 (*a*) Typical current signal from bR in PM attached to a BLM. Conditions: 26°C; 0.2 M KCl; 5 mM HEPES pH7; membrane area = 1 mm², average of 216 signals, time after membrane formation = 1 h. (*b*) Numerical integration of the signal shown in *a* after subtraction of the passive component (see text). (*c*) Voltage signal from bR. The arrows mark the two passive system discharge components at 150 ms and 1.2 s. The ratio of the slopes is 7.8. Conditions: 26°C, 0.15 M KCl, 5 mM HEPES pH7, 100 scans, time after formation = 22 h.

inflection indicating distinct processes. Polarity refers to the cytoplasmic side. The registration of the very fast inward process known from the current signal was limited by the rise time of the transient recorder. In voltage signals it was only seen at high flash light intensities (>0.5 mJ/cm²) where its relative amplitude was found to be ~3% of the outward displacement. In current measurements it was more prominent due to its small time constant. In the 20 μs and 10 ms regions two outward components are clearly seen with the amplitude of the slower component being at least two times larger than the faster one. The following two passive discharge components of the system have time constants of ~0.15 and 1.2 s and are of opposite sign having an amplitude ratio of ~8. The point of inflection of the slower active pumping component is markedly shifted to smaller values, when the first passive system component is of the same order of magnitude. The method of graphical evaluation gives thus no correct results (Nagle, 1981). So the passive system components have to be taken properly into account.

3. Characterisation of the Measuring System

Our measuring system can be described as PM fragments bound to the supporting black membrane by electrostatic forces as illustrated in Fig. 2 *a*. The extracellular side binds preferentially to the supporting membrane resulting in a net orientation of the purple membranes (Bamberg et al., 1979). After flash excitation protons are pumped through the bR from the bath into the junction between PM and BLM thus charging the membrane system. The supporting membrane has a very low conductance of ~10 nS/cm². Dipole changes within the bR molecules can also charge the membrane system, so the amplitudes of the photoelectric signal do not necessarily reflect distances of the proton displacement. Under current clamp conditions a voltage drop over the system builds up proportional to the charge displacement. This charge movement can be monitored directly by voltage measurements between the two compartments. In current measurements the system is discharged through the low input impedance of the current-voltage converter with a time constant of a few microseconds. Under these conditions the velocity of the charge movement is measured. In voltage measurements this discharge is very slow due to the large impedance of the electrometer amplifier and the backflow of charge out of the junction between the PM sheets and the BLM becomes another detectable component.

The electrical behavior of the system can be explained by the equivalent circuit shown in Fig. 2 *b*. The proton

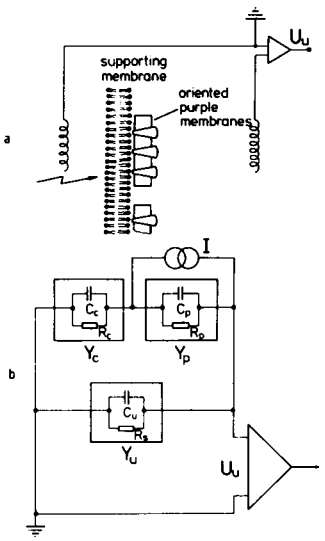

FIGURE 2 (*a*) Schematic representation of the BLM with attached PM fragments, the flash enters from the left. (*b*) Equivalent circuit of this system. Y_p is the complex admittance of the attached purple membranes, Y_c and Y_u refer to the covered and uncovered area of the bilayer membrane. R_s is the input resistance of the amplifier. I is an ideal current generator. R_p should be considered as the parallel combination of the resistance of the gap between the supporting and the purple membrane and the resistance through the PM.

pump is assumed to be an ideal current generator. The pump current I is divided by the two admittances of the PM (Y_p) and the covered area of the BLM (Y_c) and shunted by the amplifier and the capacitance of the uncovered area of the BLM (Y_u).

Circuit analysis of this system by inverse Laplace transform methods (Appendix) gives a sum of three exponentials as the response function to an exponential current input:

$$U(t) = A_0 \cdot e^{-k_0 \cdot t} + A_1 \cdot e^{-k_1 \cdot t} + A_2 \cdot e^{-k_2 \cdot t} \qquad (2)$$

with

$$A_0 = \frac{j_o \cdot x}{c_p} \cdot \frac{k_0}{(k_0 - k_1) \cdot (k_2 - k_0)}$$

$$A_1 = \frac{j_o \cdot x}{c_p} \cdot \frac{k_1}{(k_0 - k_1) \cdot (k_1 - k_2)}$$

$$A_2 = \frac{j_o \cdot x}{c_p} \cdot \frac{k_2}{(k_1 - k_2) \cdot (k_2 - k_0)}$$

where j_0 is the current density in the PM x is the fraction of the BLM area covered with PM fragments ($0 < x < 1$) and c_p is the specific capacitance of the PM. The k_i's denote the rate constants. k_0 is the rate constant of the input function, the other two correspond to the passive discharge components of the system. Assuming a very small percentage of area of the BLM being covered with purple membrane sheets ($x \ll 1$) the rate constants of the two exponentials are (see Appendix):

$$k_1 = \frac{1}{A \cdot R_s \cdot c} \qquad k_2 = \frac{g_p}{c_p + c}, \qquad (3)$$

where c denotes the specific capacitance of the BLM, c_p is the specific capacitance of the PM. g_p is the specific conductance of the PM and the conductance of the gap between PM and BLM normalized with respect to the membrane area. This is thus not a real specific quantity since it depends on the size of the PM fragments. R_s is the shunt resistor and A is the membrane area. In our experiments c was 0.5 ± 0.1 $\mu F/cm^2$ (obtained from capacitance measurements on 8 membranes) in good agreement with reported values (Fahr et al., 1981). It should be noted that k_2 only depends on specific membrane properties, whereas k_1 is affected by the shunt resistance parallel to the system. The rate constant k_0 can be assumed to be any apparent rate constant of the bR pumping being in the range of 20 s^{-1} to $10^5 s^{-1}$. In voltage measurements high R_s values are chosen, so k_1 is ~ 2 s^{-1}, therefore the photoresponse of the system can be approximated by ($k_0 \gg k_1, k_2$)

$$U(t) = \frac{j_o \cdot x}{c_p}\left[-\frac{1}{k_0} \cdot e^{-k_0 \cdot t} + \frac{k_1}{k_0 \cdot (k_1 - k_2)} \cdot e^{-k_1 \cdot t} - \frac{k_2}{k_0 \cdot (k_1 - k_2)} \cdot e^{-k_2 \cdot t}\right] \qquad (4)$$

If the input current can be described as a sum of exponentials, then the complete output function will be the sum of the corresponding output functions.

The first exponential is the integral over the input current component. The second and third components are predicted to be of opposite sign as is indeed the case experimentally (Fig. 1 *c* arrows). According to Eq. 4 their amplitude ratio should equal $-k_1/k_2$. From the slopes in Fig. 1 *c* we obtain an amplitude ratio of 7.8 which is in good agreement with the ratio of the rate constants of 8.0 ($k_1/k_2 = 1.2$ s/0.15 s). This agreement holds also in other experiments.

For current measurements R_s is very small (0.1–1 kOhm), so the system response rate constant k_1 (typ. 10^5–10^6 s^{-1}) is larger than k_0 but still of the same order of magnitude, so that the amplitude of the first exponential is no longer independent of k_1 for pumping components in the microsecond range. A clear separation from the passive system behavior is thus impossible for current measurements. Components slower than the system time constant $\tau_1 = 1/k_1$ are markedly reduced in amplitude. The photocurrent amplitudes decay to the experimental noise level in times of ~10 ms (Fig. 1 *a*), whereas photovoltage components with time constants of ~3 s are still well resolved (Fig. 1 *c*).

To test the predicted proportionality between k_1 and $1/R_s$ (Eq. 3) various resistors were inserted between the electrodes in a voltage measurement. In this experiment we purposely used 1 M KCl which gives poor attachment of the PM to the BLM, so the percentage of area being covered with PM was very low ($x \ll 1$) and Eq. 3 was expected to hold. The signal amplitude, when normalised to the flash intensity, was 20 times smaller than in our best experiments with low salt concentrations. A linear relationship between k_1 and $1/R_s$ was indeed observed as shown in Fig. 3. From the slope and the value of A an average capacitance of 0.51 ± 0.15 $\mu F/cm^2$ was calculated in agreement with the value obtained from our capacitance measurements on BLM. The apparent time constant and amplitude of the slowest component of the active bR pumping signal decreased when R_s was smaller than 33 MOhm. In all our experiments we thus used a shunt resistor of at least 100 MOhm leading to k_1 of the order 2 s^{-1}.

4. Data Evaluation With Discrete First Order Kinetics

We have fitted the signals with a sum of exponentials using the program DISCRETE (Provencher, 1976 *a*, *b*), which fits up to 9 exponentials plus a nonzero baseline. Voltage signals required usually 7 to 9 components including the two passive-system time constants. The pumping process was thus described by at least 5 exponentials which, however, were poorly reproducible between different membranes under identical conditions. This is clearly seen in the Arrhenius diagram (Fig. 4). The factor between subsequent time constants was always ~5–6 covering a range

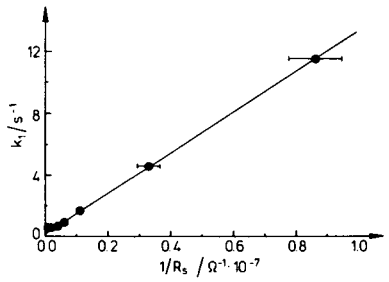

FIGURE 3 Dependence of the rate constant of the fast system discharge on the reciprocal of the shunt resistance. The straight line is a linear regression yielding a capacitance of 7.6 nF. Membrane area was 0.015 ± 0.003 cm^2. The accuracy of the resistors was 10%.

from about 5 μs to ~20–30 ms. Within a single experiment the temperature dependence was rather linear (filled circles) but the components cannot be associated with each other between different membranes (other symbols). Approaches to fit the data with less than five exponentials led always to deviations exceeding the noise level (Fig. 5, *a* and *b*). The results were sensitive for changes in the number of time decades and for the start time value used for the fit. Together with the considerable scatter of results from other authors (see discussion) these findings indicate that either the system behaves irreproducibly, or the description with first order kinetics is not suitable. An indication in favor of the latter assumption was obtained from appropriate plots of the components derived from DISCRETE fits. The relative photovoltage amplitudes normalized to 100% were plotted as a function of their corresponding time constants. When this is done with the results of DISCRETE fits to the same signal with different numbers of exponentials (Fig. 5 *f* symbols) it is seen that the data points concentrate around three peak values suggesting that a description with a continuous relaxation time spectrum might be more reasonable.

5. Data Evaluation With a Model of Distributed Kinetics

Distributed relaxation time constants are expected if the activation energy E_A of the barriers for the individual

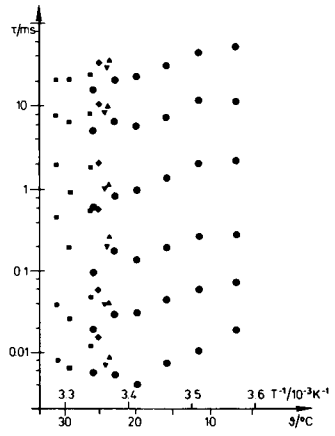

FIGURE 4 Arrhenius diagram of the time constants obtained from 6-exponential fits. The different symbols refer to different membranes under identical conditions (5 experiments).

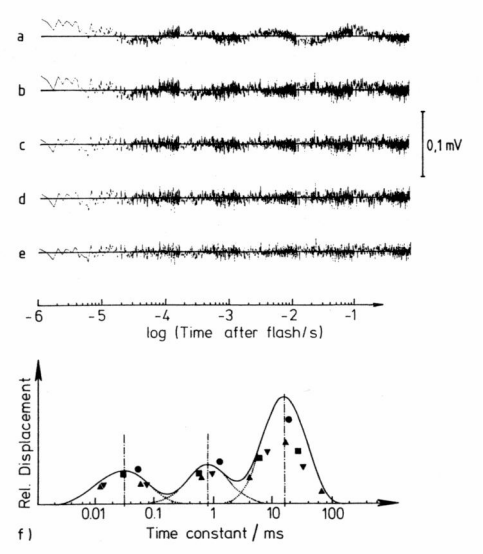

FIGURE 5 (*a–d*); Residuals of DISCRETE fits to a photovoltage signal with 3, 4, 5, and 6 exponentials. (*e*); Residuals of CONTIN fits (continuous relaxation time spectrum) of the same signal. (*f*); Plot of the relative amplitudes of the above DISCRETE fits with a sum of 3(●), 4(■), 5(▼), and 6(▲) exponentials as a function of their corresponding time constants. Straight line: Continuous relaxation time spectrum obtained from CONTIN. The dotted lines are drawn to guide the eye. The peak time constants are 30 μs, 0.8 ms, and 15 ms. The amplitude ratios are 21, 19, and 60%. Conditions: 25°C, 0.15 M KCl, 5 mM HEPES pH7, 8 scans. 16 min after membrane formation.

proton translocation steps are slightly different from molecule to molecule depending on the "conformational substate" the molecule occupies at the time of pumping (Austin et al., 1975). The relative number N of protons having passed the energy barrier at a time t is thus given by

$$N(t) = N_0 \cdot \int_0^\infty g(E_A) \cdot \exp[-k(E_A) \cdot t] \cdot dE_A. \quad (5)$$

The $g(E_A)$ is the distribution function of the activation energy and $k(E_A)$ is the corresponding rate constant. To test the model we have used the program CONTIN (Provencher, 1982a–c), which has been especially designed for fitting continuous relaxation time spectra to kinetic data. To obtain the displacement distribution function $g(E_A)$ the equation

$$U(t) = U_0 \cdot \int_{k1}^{k2} g[\ln(k)] \cdot \exp[-k(E_A) \cdot t] \, d\ln(k) \quad (6)$$

was fitted to the photovoltage signals in a fixed grid in $\ln(k)$. The integration was done over $\ln(k)$ because $k(E_A)$ is expected to follow $k = A \cdot \exp(-E_A/R \cdot T)$. The integration interval was restricted to the range from 10 s^{-1} to 10^6 s^{-1} covering the range of our experimental data. For such a problem there is an infinite number of solutions (Provencher and Dovi, 1979), but to obtain a spectrum with a reasonably small number of peaks CONTIN uses the principal of parsimony: It searches for the "smoothest" solution by minimizing the second differences of the spec-

trum $g(\ln(k))$ until the mean standard deviation of the fit clearly exceeds experimental noise. The integration was done over 80 fixed grid points which was sufficient since reducing the number of points to 40 gave similar results. To avoid oscillations in the solutions the nonnegativity constraint for $g(\ln(k))$ was found to be necessary. First we subtracted the passive discharge components using the fit results from DISCRETE. After this separation the remaining bR pumping signal (Fig. 6) could be used for graphical evaluation, which gave two components with $\tau_{fast} = 25 \pm 4$ μs and $\tau_{slow} = 14 \pm 2$ ms, where the slower component makes up 75 ± 3 percent of the total signal amplitude (obtained from 9 measurements on 5 membranes). The typical spectrum obtained from CONTIN (Fig. 5 *f* solid line) shows a third component in the 1 ms range which is detectable in the signal by eye only at high signal to noise ratios. The spectrum confirms the results of the distributed plot of the components obtained from DISCRETE fits (Fig. 5 *f*, symbols). The three components are well reproducible and the mean standard deviation of the fit is equal to that of DISCRETE fit with 5 exponentials or even more (Fig. 5, *c–e*) which means that at least 11 adjustable parameters (2 for each component and 1 for the baseline) are necessary to fit the signal correctly. Tests with a CONTIN analysis constrained to two peaks failed, indicating that the middle peak is not an artifact but is really required to fit the data. CONTIN does statistical tests of the different results and calculates the goodness of fit and the degrees of freedom for all solutions. For a symmetric three peak distribution ten degrees of freedom (3 for each component and 1 for the baseline) should be expected but the real value is smaller (9 ± 1) because the regularization affects the whole spectrum equally so that the adjustable parameters for each peak cannot be determined separately. Possible small asymmetries in the distribution are not detected by CONTIN.

To characterise the distribution function numerically the different moments of the peaks were computed. A good measure for the average time constants are the peak values, which are approximately equal to the mean values in $\ln(\tau)$, which correspond to the average activation energies of the three components. These values of the time constants of the three peaks are $\tau_1 = 32 \pm 8$ μs. $\tau_2 = 890 \pm 150$ μs and $\tau_3 = 18 \pm 5$ ms. The errors are not the halfwidths of the peaks but the standard deviations of the mean values obtained from 9 measurements on 5 membranes. The ratios of the areas of the peaks are 2.0 (±0.2) : 1.5 (± 0.3) : 6.5 (±0.4). The τ_1 and τ_3 components are slightly different from those obtained from the graphical evaluation (Fig. 6). When the means are determined by integrating in equal intervals of τ instead of $\ln(\tau)$ the resulting time constants are similar to those obtained from graphical evaluation. The time constants are then ~1.3-fold smaller than those derived from averaging over $\ln(\tau)$. This factor is in agreement with the value expected for Gaussian distributions (Lindau, 1984). The temperature dependence of the peak time constants is shown in the Arrhenius diagram (Fig. 7) which yields activation energies of $E_{A1} = 57 \pm 15$ kJ/mol, $E_{A2} = 52 \pm 10$ kJ/mol and $E_{A3} = 44 \pm 10$ kJ/mol in rough agreement with reported values (Rayfield, 1985). The amplitude ratios change to 4:2:4 at 5°C. The halfwidths of the peaks show a clear tendency towards larger values for the fastest component (0.9 ± 0.1 decades) and 0.7 ± 0.2 decades for the other two peaks. No significant temperature dependence of the halfwidths was found. The spectrum was unchanged, when high flash intensities (1.5 mJ/cm²) were used.

To test whether the results from voltage and current measurements are equivalent, we did both measurements on the same membrane. The continuous relaxation time spectra from both measuring methods on the same mem-

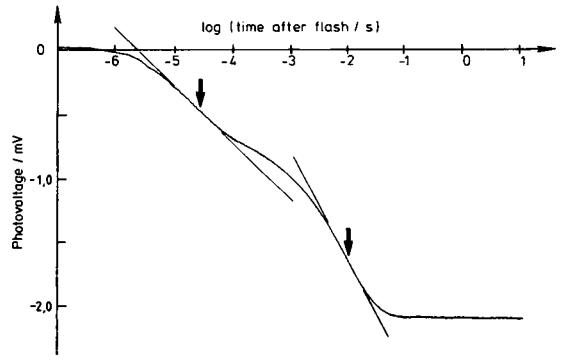

FIGURE 6 The signal of Fig. 1 *c* after subtraction of the passive discharge components obtained from DISCRETE (0.21 s/2.24 mV and 1.56 s/0.244 mV). The inflection points (*arrows*) are at 28 μs and 11 ms. The slower component contributes 67% of the total charge displacement.

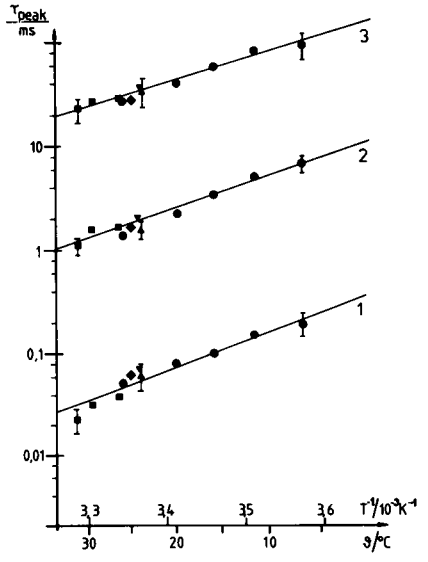

FIGURE 7 Arrhenius diagram of the peak time constants obtained from fits with a continuous relaxation time spectrum. The activation energies were calculated by linear regression (*straight lines*) yielding from the fastest to the slowest component: $E_{A1} = 57 \pm 15$ kJ/mol, $E_{A2} = 52 \pm 10$ kJ/mol, and $E_{A3} = 44 \pm 10$ kJ/mol.

brane (Fig. 8) are similar within experimental error which is rather large for the slowest component of the current signal due to the small amplitude in the late signal. For fitting the spectrum to the current signal we changed the integrand in Eq. 5 to obtain the displacement distribution $g(\ln(k))$:

$$I(t) = I_0 \int_{k1}^{k2} k \cdot g\,[\ln(k)] \cdot e^{-k \cdot t}\, d\ln(k) \qquad (7)$$

As an additional result we found that the τ_1 peak was markedly affected by the high salt concentration of 1M KCl, which we used to get a small system time constant in the current measurements. The peak τ values of the spectra were $\tau_1 = 71 \pm 5$ μs, $\tau_2 = 1.0 \pm 0.1$ ms and $\tau_3 = 19 \pm 3$ ms, the amplitude ratio was the same as with 150mM KCl. This result was confirmed in 13 separate experiments on three membranes.

DISCUSSION

The above results show that current clamp is the method of choice to investigate the whole time range of electric events during the bR photocycle, since the photovoltage directly follows the time course of the charge displacement. From the first large charge movement to the complete relaxation of the membrane system eight decades of time are required. Thus data registration with a fixed sampling rate is not applicable as this may lead to erratic results, when fit programs are used which require equally weighted data points. We solved this problem by using a quasilogarithmic clock. A similar technique has been applied to study the distributed kinetics of ligand rebinding to myoglobin (Austin et al., 1975).

A detailed equivalent circuit analysis of the whole membrane system is necessary to separate active charge movement from the passive relaxation processes. The signal shaping by the membrane system was not accounted for in most of the previous work. The slow system discharge components described here confirm the validity of the equivalent circuit of Fig. 2 *b* for the experimental system.

Previous results scatter widely with respect to the number of components as well as to their corresponding time constants and amplitudes (Table I). It is difficult to compare the results since with one exception (Drachev et al., 1978) no experimental errors are given. The variability of the results indicates, however, that either the different measuring systems affected the pumping behavior, or the data evaluation was not adequate. All results show in common a fast inward charge movement followed by outward steps with time constants from 15 μs to 33 ms, where the slowest component is the largest. We have shown that voltage- and current clamp measurements yield equivalent displacement time courses, so the results from both measuring methods should be in agreement.

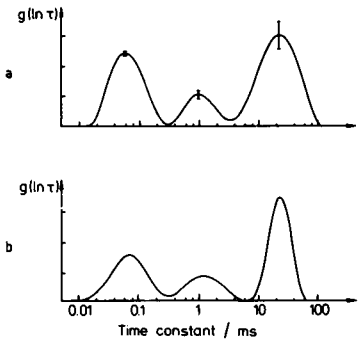

FIGURE 8 Relaxation time spectra obtained from *a* current (394 scans) and *b* voltage (194 scans) measurements on the same membrane. 22°C, 1 M KCl, 5 mM HEPES pH7, Ag-AgCl electrodes for both measurements.

Techniques using suspensions or gels containing PM fragments allow only current measurements since the system discharge time constant is very fast. Because of the resulting small amplitude in the slow components of the current signal two authors did not detect the components in the 10 ms range which contribute 70–75% of the total displacement amplitude (Der et al., 1984; Fahr et al., 1981). The reported values of time constants and amplitudes in that time range deduced from current measurements should thus be considered with caution (Keszthelyi and Ormos, 1980; Ormos and Keszthelyi, 1985).

The results of graphical evaluation of voltage measurements are in rather good agreement even between data from different experimental techniques. They have in common a component with ~70–75% of the total charge displacement in the 10–20 ms range and another component at ~25 μs. However, the results of 3-exponential fit programs yielding an additional component in the ms range scatter widely, even when the same technique was used, indicating that not the measuring technique but the data evaluation method is inadequate. Our results might explain the observed multiplicity of exponential components in terms of a distributed kinetics model, which reveals three processes of outward charge movement during the photocycle. Application of our model to other measuring techniques may lead to different parameter values for the three components depending on the local environment of the bR molecules in the specific experimental arrangement. But despite this the peak time constants reported here are in rough agreement with the results of other workers, who used three exponenetial fits for data evaluation (Rayfield, 1983, 1985; Drachev et al., 1980). This is not surprising, since fits of the spectrum with a sum of <5 exponentials tend to converge to the peak values of the three distribution peaks but give excessively large fit deviations (see Fig. 5 *a*, *f*) and must thus be rejected as an incomplete description. A time constant spectrum like that shown in Fig. 5 *f* was obtained in all experiments under the same conditions, so we now have a standard data base of good reproducibility upon which further investigations can be based. Only if the native state is electrically characterised with sufficient reliability can measurements on chemically or genetically modified bR give meaningful results

TABLE I
PREVIOUSLY PUBLISHED TIME CONSTANTS AND AMPLITUDES OF PHOTOELECTRIC SIGNALS*

Reference	$\tau_0/\mu s$	$\tau_1/\mu s$	$A_1/\%$	τ_2/ms	$A_2/\%$	τ_3/ms	$A_3/\%$	Temp °C
Voltage clamp methods:								
1)	<1.0	30, 89		3.4				25
2)	1.2	17, 57		0.95				25
3)	<5.0	30		1.4		5.4		22
4)	4.4	81	10	2.5	29	8	61	20
Current clamp methods:								
5)	<0.002	115	29			4.5	71	?
6)	<0.3	25–50	25			6–12	75	?
7)	<0.2	14, 68	20	3.6	12	11	68	26
8)	<1.0	57	10	1.06	16	13	74	23
9)	<1.0	38	20	2.4	21	33	59	20
10)	<1.0	25	26			18	74	20
11)	<0.3	32 ± 8	20 ± 2	0.89 ± .15	15 ± 3	18 ± 5	65 ± 4	25
12)	<0.3	25 ± 4	25 ± 3			14 ± 2	75 ± 3	25

*For clarity the time constants were grouped tentatively. 1) Der et al., 1984; 2) Fahr et al., 1981; 3) Fig. 3 of Ormos and Keszthelyi, 1985; 4) Keszthelyi and Ormos, 1980; 5) Trissl, 1983; 6,7) Drachev et al., 1978, 1980; 8,9) Rayfield 1983, 1985; 10) Fig. 1 of Rayfield, 1986 evaluated graphically; 11,12) Results of this work from the peak time constants and the graphical evaluation respectively.

from which a deeper understanding of the mechanism of the proton pump may be obtained.

As discussed in paragraph three of the Results section we always provided for large passive time constants, being at least one order of magnitude larger than the slowest active pumping time constant, by choosing high shunt resistors. So we could be sure that the active system response was not affected by artifacts of the discharge behavior even for the "slower tail" of the third bR pumping component.

The electrical parameters c, c_p, and g_p of the measuring circuit are specific quantities normalized with respect to the membrane area. Of these quantities g_p is expected to be distributed since it depends on the diameters of the attached PM patches which show a wide distribution. This is well known from electron micrographs of PM suspensions. We therefore tested whether the system time components are really exponentials by fitting distributions to them. The large negative system component has a halfwidth of <0.2 decades, the slower component is somewhat broader. When we subtracted the passive system components as distributed functions instead of two exponentials before doing the CONTIN analysis no change in the resulting peak time constants and amplitudes of the active charge displacement was obtained. The exponential approximation of the passive system response is thus adequate and the slightly distributed kinetics of the measuring system does not affect the kinetics of the proton pump. Having eliminated as one possible source for distributed kinetics the distribution of electrical parameters in the measuring circuit, we conclude that conformational substates offer the most likely explanation for our results.

Distributed kinetics based on conformational substates have been proposed for a variety of protein functions. The relaxation time constants of protein conformational substates range from picoseconds to seconds and are highly dependent on their local environment (Doster, 1983). A distribution of activation energies for the passage of an energy barrier (Fig. 9) emerges only, if the average lifetime of the conformational substates is larger than the time constant of this step. If the interconversion between the substates is faster, only an average activation energy is detectable as a single time constant. The crystalline lattice of the PM may be the cause of such a "freezing" of conformational substates, but preliminary experiments with monomeric bR in vesicles also showed distributed photovoltage kinetics.

The exact form of the distribution of the conformational substates is still speculative, and also the resulting activation energy distribution is unknown. However, treatment according to spin glass theory suggests that the conformational energy distribution is Gaussian having a variance of about R · T. Very good fits to flash photolysis data for recombination of CO to T-hemoglobin were obtained, if the E_A distribution was assumed to follow the distribution of initial conformational energies (Stein, 1985). The shape of the relaxation time distributions for the three photovoltage components could not be detected exactly, but it seems to be rather symmetric having halfwidth of about one decade. This might be approximated by a Gaussian activation energy distribution with a variance of about R · T as expected for the distribution of conformational substates (Stein, 1985). Fig. 9 shows a model where the height of the barrier is fixed and the energy of the initial states is distributed according to a slow thermal equilibrium. This model suggests, that the individual charge displacement steps are a consequence of conformational changes. The protein is trapped in a conformational state

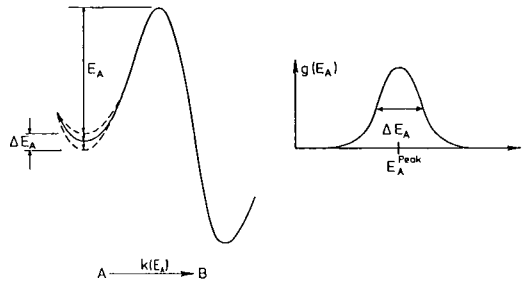

FIGURE 9 Distributed initial energies of conformational substates lead to a distribution of activation energies. The halfwidth is in the order of R · T.

and has to enter a more flexible transition state before the charge movement is possible. The switching of proteins between defined conformational substates and a flexible transition state has been observed in deoxymyoglobin crystals with Mössbauer spectroscopy (Parak et al., 1982). The high activation energies obtained for the peak rate constants also support the involvement of considerable conformational changes in the three charge movements.

The comparison of the kinetics of the light-induced photovoltage signals with spectroscopically defined intermediates is still difficult, since photocycle measurements cannot be done simultaneously on the BLM-PM system due to the small number of bR molecules generating the electric signal. A comparison with photocycle data obtained in suspensions suffers from the fact that the local environment of PM fragments attached to a BLM differs from that of fragments in suspension. On the other hand there is no need for a direct correspondence between electrogenic events and photocycle components since the absorbance changes are only caused by local interactions of the chromophore while the photovoltage measurement is sensitive to charge movements and conformational changes within the whole protein. The distributive behavior, however, seems to be a common feature of both cycles (Xie et al., 1985; Groma and Dancshazy, 1986, own measurements), whereas the time constants of the components are in poor agreement.

The 32 μs component might be correlated with the appearance of the M_{412} intermediate which is associated with the proton release at the extracellular side of the membrane (Ort and Parson, 1978; Grzesiek and Dencher, 1986). The slowest component may be associated with the rebinding of the proton from the cytoplasmic side during the return to the bR_{568} groundstate. The displacement peak at 890 μs has no obvious optical counterpart.

APPENDIX

Laplace Transform Equivalent Circuit Analysis

The equivalent circuit of the system is shown in Fig. 2 *b*. The light-induced displacement current I is split according to:

$I = I_p + I_c$ with $I_p = U_p \cdot Y_p$ and

$$I_c = U_p \cdot \frac{Y_c \cdot Y_u}{Y_c + Y_u} = U_u \cdot Y_u \quad \text{(A1)}$$

where $Y = G + s \cdot C$ are the complex admittances ($s = i \cdot \omega$). We obtain

$$I = U_p \cdot \left(Y_p + \frac{Y_c \cdot Y_u}{Y_c + Y_u}\right) \text{and the measured voltage} \quad \text{(A2)}$$

$$U_u = I \cdot \frac{Y_c}{Y_p \cdot Y_c + Y_p \cdot Y_u + Y_u \cdot Y_c} \quad \text{(A3)}$$

Since the admittances depend linearly on the percentage of the membrane area which is covered with PM fragments, they can be written in terms of specific values (indicated by small letters): $Y_p = x \cdot A \cdot y_p$, $Y_c = x \cdot A \cdot y$ and $Y_u = 1/R_s + (1 - x) \cdot A \cdot y$, where A is the area of the membrane (here 0.015 cm^2) and x is the fraction of the membrane area covered with PM ($0 < x < 1$). y is the specific admittance of the BLM assumed to be unchanged in areas covered with PM. Neglecting the conductance of the BLM (typ.10 ns/cm^2) only its capacitive part remains: $y = s \cdot c$ with c being the specific capacitance of the BLM (0.5 μF/cm^2). The specific admittance of the PM is $y_p = g_p + S \cdot c_p$ with g_p and c_p being the composite specific conductance and the specific capacitance of the PM respectively.

In the frequency domain the photovoltage is given by

$$U_u(s) = \frac{I(s)}{A \cdot c_p} \cdot \frac{s}{s^2 \cdot \left[(1-x) \cdot \frac{c}{c_p} + 1\right] + s \cdot \left[\frac{g_p}{c_p} + \frac{1}{A \cdot R_s} \cdot \frac{c + c_p}{c \cdot c_p}\right] + \frac{1}{A \cdot R_s \cdot c} \cdot \frac{g_p}{c_p}} \quad \text{(A4)}$$

The Laplace transform of an exponentially decaying current

$$I(t) = I_0 \cdot e^{-k_0 \cdot t} \quad \text{is} \quad I(s) = \frac{I_0}{s + k_0} \quad \text{(A5)}$$

The current amplitude is expected to be a linear function of the total area of the attached PM sheets: $I_0 = j_0 \cdot x \cdot A$, where j_0 denotes the current density in the PM. In the frequency domain the voltage is thus of the common form

$$U_u(s) = \frac{j_0 \cdot x}{c_p} \cdot \frac{s}{(s + k_0) \cdot (s + k_1) \cdot (s + k_2)}. \quad \text{(A6)}$$

Inverse Laplace transform of this expression leads to the

time course of the photovoltage:

$$U(t) = A_0 \cdot e^{-k_0 \cdot t} + A_1 \cdot e^{-k_1 \cdot t} + A_2 \cdot e^{-k_2 \cdot t} \qquad \text{(A7)}$$

$$\text{with } A_0 = \frac{j_0 \cdot x}{c_p} - \frac{k_0}{(k_0 - k_1) \cdot (k_2 - k_0)}$$

$$A_1 = \frac{j_0 \cdot x}{c_p} - \frac{k_1}{(k_0 - k_1) \cdot (k_1 - k_2)}$$

$$A_2 = \frac{j_0 \cdot x}{c_p} - \frac{k_2}{(k_1 - k_2) \cdot (k_2 - k_0).}$$

The measured signal contains two passive system components with the rate constants k_1, k_2 being the negative poles of the frequency domain formula.

The roots of the quadratic equation of the denominator yield

$$k_{1,2} = \frac{k_p + k_u + k_{up}}{2 \cdot [(1 - x) \cdot c/c_p + 1]} \pm \frac{\sqrt{(k_p + k_u + k_{up})^2 - 4 \cdot k_p \cdot k_u \cdot [(1 - x) \cdot c/c_p + 1]}}{2 \cdot [(1 - x) \cdot c/c_p + 1]} \qquad \text{(A8)}$$

with $k_p = g_p/c_p$, $k_u = 1/(A \cdot R_s \cdot c)$ and $k_{up} = 1/(A \cdot R_s \cdot c_p)$. For $x \ll 1$ the passive rate constants can be approximated by

$$k_1 = \frac{1}{A \cdot R_s \cdot c} \qquad \text{and, } k_2 = \frac{g_p}{c + c_p}. \qquad \text{(A9)}$$

We thank Dr. Alfred Fahr for developing the experimental apparatus, Wolfgang Nitschke, Jürgen Kleindienst, and Marian Luft of the electronic workshop for the design and construction of the logarithmic time base, and Ingrid Wallat for the preparation of the purple membranes.

This work was supported by the Deutsche Forschungsgemeinschaft (Sfb. 312,B1).

Received for publication 30 July 1987 and in final form 8 December 1987.

REFERENCES

Alcala, J. R., E. Gratton, and F. G. Prendergast. 1987. Fluorescence lifetime distributions in proteins. *Biophys. J.* 51:597–604.

Alcala, J. R., E. Gratton, and F. G. Prendergast. 1987. Interpretation of fluorescence decays in proteins using continuous lifetime distributions. *Biophys. J.* 51:925–936.

Austin, R. H., K. W. Beeson, L. Eisenstein, H. Frauenfelder, and I. C. Gunsalus. 1975. Dynamics of ligand binding to myoglobin. *Biochemistry.* 14:5355–5373.

Bamberg, E., H.-J. Apell, N. A. Dencher, W. Sperling, H. Stieve, and P. Läuger. 1979. Photocurrents generated by bacteriorhodopsin on planar bilayer membranes. *Biophys. Struct. Mech.* 5:277–292.

Braunstein, D., M. K. Kyung, S. L. Lin, P. Ormos, and J. Vittitow. 1987. Inhomogeneous broadening in the absorption spectrum of bacteriorhodopsin. *Biophys. J.* 51:135. (Abstr.)

Der, A., P. Hargittai, and J. Simon. 1985. Time-resolved photoelectric and absorption signals from oriented purple membranes immobilized in gel. *J. Biochem. Biophys. Methods.* 10:295–300.

Doster, W. 1983. Viscosity scaling and protein dynamics. *Biophys. Chem.* 17:97–103.

Drachev, L. A., A. D. Kaulen, and V. P. Skulachev. 1978. Time resolution of the intermediate steps in the bacteriorhodopsin-linked electrogenesis. *FEBS (Fed. Eur. Biochem. Soc.) Lett.* 87:161–167.

Drachev, L. A., A. D. Kaulen, V. Khitrina, and P. Skulachev. 1981. Fast stages of photoelectric processes in biological membranes. *Eur. J. Biochem.* 117:461–470.

Fahr, A. 1981. Photoelektrische Untersuchungen von Bacteriorhodopsin an künstlichen Lipidmembranen: eine kinetische analyse. Thesis, University of Konstanz, FRG.

Fahr, A., P. Läuger, and E. Bamberg. 1981. Photocurrent kinetics of purple-membrane sheets bound to planar bilayer membranes. *J. Membr. Biol.* 60:51–62.

Groma, G. I., and Zs. Dancshazy. 1986. How many M forms are there in the bacteriorhodopsin photocycle? *Biophys. J.* 50:357–366.

Grzesiek, S., and N. A. Dencher. 1986. Time-course and stoichiometry of light-induced proton release and uptake during the photocycle of bacteriorhodopsin. *FEBS (Fed. Eur. Biochem. Soc.) Lett.* 208:337–342.

Keszthelyi, L., and P. Ormos. 1980. Electric signals associated with the photocycle of bacteriorhodopsin. *FEBS (Fed. Eur. Biochem. Soc.) Lett.* 19:189–193.

Lindau, M., and H. Rueppel. 1983. Evidence for conformational substates of rhodopsin from kinetics of light-induced charge displacements. *Photobiochem. Photobiophys.* 5:219–228.

Lindau, M. 1984. Lichtinduzierte Ladungsbewegungen des Rhodopsins. Thesis, Technical University Berlin.

Marrero, H., and K. J. Rothschild. 1987. Conformational changes in bacteriorhodopsin studied by infrared attenuated total reflection. *Biophys. J.* 52:629–635.

Nagle, J. F. 1981. Upon the optimal graphical representation of flash data from photochemical systems obeying first order kinetics. *Photochem. Photobiol.* 33:937–939.

Ormos, P., S. Hristova, and L. Keszthelyi. 1985. The effect of pH on proton transport by bacteriorhodopsin. *Biochim. Biophys. Acta.* 809:181–186.

Ort, D. R., and W. W. Parson. 1978. Flash-induced volume changes of bacteriorhodopsin-containing membrane fragments and their relationship to proton movements and absorbance transients. *J. Biol. Chem.* 253:6158–6164.

Parak, F., E. W. Knapp, and D. Kucheda. 1982. Protein dynamics. Mössbauer spectroscopy on deoxymyoglobin crystals. *J. Mol. Biol.* 151:177–194.

Provencher, S. W. 1976a. A fourier method for the analysis of exponential decay curves. *Biophys. J.* 16:27–41.

Provencher, S. W. 1976b. An eigenfunction expansion method for the analysis of exponential decay curves. *J. Chem. Phys.* 64:2772–2777.

Provencher, S. W., and Dovi, V. G. 1979. Direct analysis of continuous relaxation spectra. *J. Biochem. Biophys. Methods.* 1:313–318.

Provencher, S. W. 1982a. A constrained regularization method for inverting data represented by linear algebraic or integral equations. *Comput. Phys. Commun.* 27:213–227.

Provencher, S. W. 1982b. CONTIN: A general purpose constrained regularization program for inverting noisy linear algebraic and integral equations. *Comput. Phys. Commun.* 27:229–242.

Provencher, S. W. 1982c. CONTIN Users Manual. EMBL Technical Report DA05.

Rayfield, G. W. 1983. Events in proton pumping by bacteriorhodopsin. *Biophys. J.* 41:109–117.

Rayfield, G. W. 1985. Temperature dependence of photovoltages generated by bacteriorhodopsin. *Biophys. J.* 48:111–115.

Rayfield, G. W. 1986a. Evidence for distributed barrier heights in bacteriorhodopsin. *Biophys. J.* 49:209. (Abstr.)

Rayfield, G. W. 1986b. Evidence that charge motion within bacteriorhodopsin depends on solvent viscosity. *Photochem. Photobiol.* 43:171–174.

Stein, D. L. 1985. A model of protein conformational substates. *Proc. Natl. Acad. Sci. USA.* 82:3670–3672.

Stoeckenius, W., R. H. Lozier, and R. A. Bogomolni. 1979. Bacteriorhodopsin and the purple membrane of halobacteria. *Biochim. Biophys. Acta.* 505:215–278.

Trissl, H. W. 1983. Charge displacements in purple membranes absorbed to a heptane/water interface. *Biochim. Biophys. Acta.* 723:327–331.

Varo, G., and L. Keszthelyi. 1983. Photoelectric signals from dried oriented purple membranes of *Halobacterium halobium*. *Biophys. J.* 43:47–51.

Xie, A., R. H. Lozier, and R. A. Bogomolni. 1986. Halorhodopsin photocycle studies. *Biophys J.* 49:209. (Abstr.)

Xie, A. H., J. F. Nagle, and R. H. Lozier. 1985. Bacteriorhodopsin photocycle: distributed kinetics analysis of flash photolysis absorbance data. *Biophys. J.* 47:98. (Abstr.)